CONTRAST MEDIA & MOLECULAR IMAGING
Contrast Media Mol. Imaging **2**:240–247 (2007)
Published online 3 December 2007 in Wiley InterScience (www.interscience.wiley.com) DOI:10.1002/cmmi.150

CONTRAST MEDIA & MOLECULAR IMAGING

Full Paper

Reporter gene imaging using radiographic contrast from nonradioactive iodide sequestered by the sodium–iodide symporter

Stephen L. Brown[1], Svend O. Freytag[1], Kenneth N. Barton[1], Michael J. Flynn[2], Donald J. Peck[2], Aleksandar F. Dragovic[1], Ryan Jin[1], Yener N. Yeni[3], David P. Fyhrie[3], Clifford M. Les[3], Guopei Zhu[1], Andrew Kolozsvary[1], Wayne C. Pitchford[4], S. David Nathanson[5], Joseph D. Fenstermacher[4] and Jae Ho Kim[1]*

[1]*Department of Radiation Oncology, Henry Ford Health System, Detroit, MI 48202, USA*
[2]*Department of Radiology, Henry Ford Health System, Detroit, MI 48202, USA*
[3]*Department of Orthopedics, Henry Ford Health System, Detroit, MI 48202, USA*
[4]*Department of Anesthesiology, Henry Ford Health System, Detroit, MI 48202, USA*
[5]*Department of Surgery, Henry Ford Health System, Detroit, MI 48202, USA*

Received 24 April 2007; Revised 31 August 2007; Accepted 7 October 2007

ABSTRACT: The hypothesis that the human sodium–iodide symporter, NIS, can be used to detect NIS expression using standard radiological techniques was tested using adenoviral transduced NIS expression in human tumor xenografts grown in mice and in a naive dog prostate. Nonradioactive iodide was administered systemically to animals that 1–3 days previously had received a local injection of a replication-competent adenovirus expressing NIS under the control of the CMV promoter. The distribution of radiopacity was assessed in mouse tumors using micro-CT and a clinical X-ray machine and in the prostate of an anesthetized dog using a clinical spiral CT. Iodide sequestration and NIS expression were measured using X-ray spectrochemical analysis and fluorescence microscopy, respectively. Radiographic contrast due to NIS gene expression that was observed indicates the technique has potential for use in preclinical rodent tumor studies but probably lacks sensitivity for human use. Copyright © 2007 John Wiley & Sons, Ltd.

KEYWORDS: sodium–iodide symporter; nonradioactive radiographic contrast; reporter gene imaging

INTRODUCTION

The diagnostic potential of X-rays to noninvasively image anatomy in living systems was almost immediately realized(1) following their discovery more than 100 years ago,(2) X-rays have remained a widely used format for diagnostic imaging examinations. The benefits of X-ray attenuation imaging of anatomy provide the same justifications for exploring their use in reporter gene imaging. Radiological equipment and reporter strategies are safe, dependable and relatively inexpensive. Despite the benefits of the approach, imaging contrast using radiological attenuation has not been utilized as a gene imaging strategy.

Candidate contrast agents should be nontoxic and effectively attenuate diagnostic X-rays. One candidate contrast agent particularly appealing for X-ray attenuation imaging is iodide, which currently is routinely used as a radiographic vascular imaging contrast agent. The X-ray attenuation for iodide at photon energies commonly used in diagnostic radiology is more than an order of magnitude greater than that of carbon, oxygen, hydrogen or nitrogen,(3) which together account for more than 99% of biological material.(4) Iodide represents an ideal substrate for reporter gene imaging.

Iodide sequestration within cells is mediated by the Na–I symporter (NIS), a molecular pump identified by Carrasco and co-workers(5) using rat thyroid cells. Jhiang and co-workers cloned human NIS,(6) which has since been incorporated into gene therapy strategies as a reporter gene using radioactive iodide and anions of similar size and charge as that of iodide. The combined NIS symporter, radioactive substrate and nuclear medicine technology has been remarkably successful as a reporter gene imaging strategy. For example, at Henry Ford Health System, we recently used SPECT images to monitor NIS gene expression in a patient with localized prostate cancer three days after an intratumor injection of adenovirus. The replication-competent adenovirus expressing NIS used in the human study is the same

**Correspondence to*: S. L. Brown, Department of Radiation Oncology, Henry Ford Hospital, 2799 West Grand Blvd, Detroit, MI 48202, USA.
E-mail: sbrown1@hfhs.org
Contract/grant sponsor: National Institutes of Health; *contract/grant number:* P01CA097012 (SOF).
Abbreviations: NIS, human sodium–iodide symporter

virus as that used in the current study, so the potential to translate results of improved NIS gene imaging are real and immediate.

In this report we explore experimentally the utility of gene imaging with NIS, nonradioactive iodide and imaging contrast based on radiological attenuation. The detectability of radiographic contrast from NIS expression and iodide uptake was addressed microscopically on the cellular level using thin tissue sections and macroscopically in human tumor xenografts grown in mice and in a dog prostate. The large animal study was included to examine the ease with which the approach could be translated to routine clinical use.

METHODS AND MATERIALS

In mice and the dog, tissue was transduced with adenovirus expressing NIS, and radiographic images were obtained 1–3 days after the local injection of the virus. Radiographic contrast was assessed in mice with specimen radiography (*ex vivo*), imaging whole mice using micro-CT and a clinical X-ray machine, and in the dog using a clinical spiral CT.

Virus

Cells were transduced with AD5-yCD/mutTK$_{sr39}$ *rep*-hNIS, a replication-competent type-5 adenovirus containing the human sodium iodide symporter in the E3 region under transcriptional control of a CMV promoter as described previously(7).

Tumor cells

A549 cell lines were maintained in culture prior to tumor xenograft studies. A549 cells derived from a lung carcinoma in a 58 year-old Caucasian male (CCL-185, American Type Culture Collection, Manassas, VA, USA) were grown in Dulbecco's modified Eagle's medium with phenol red, supplemented with L-glutamine (2 mM), penicillin (100 U/ml), streptomycin (100 μg/ml) and 10% fetal bovine serum. MCF-7 breast cancer cells were used as a positive control, since most breast cancer expresses NIS endogenously. MCF-7, an estrogen-positive metastatic mammary adenocarcinoma, derived from the pleural effusion of a 69-year-old Caucasian female (HTB-22, American Type Culture Collection, Manassas, VA, USA) and was maintained under identical conditions as A549 cells except that MCF-7 cell culture media was supplemented with estradiol (1 nM).

Animal studies

Animal studies were conducted according to Association for Assessment and Accreditation of Laboratory Animal Care (AAALAC) regulations and were approved by the Henry Ford Health System Institutional Animal Care and Use Committee (IACUC).

Mice. Tumor cells (5×10^{-6} cells in 1 ml) were implanted into the gastrocnemius muscle of CD-1 *nu/nu* athymic mice half-way between the knee and ankle. Xenografts were studied 8–10 weeks after implantation when they weighted between 0.4 and 0.8 g and were 9.0–11.5 mm in diameter. Mice with A549 tumors were transduced with: (1) NIS-expressing adenovirus (Ad-NIS; $n = 8$); (2) a similar adenoviral construct lacking the NIS gene (gene control; $n = 6$); or (3) with Ad-NIS but not administered iodide (iodide control; $n = 2$). For each mouse, 10^{-8} adenoviral particles (vp) were suspended in isotonic saline (not phosphate buffered saline since phosphate gave a small but noticeable radiographic artifact; no such artifact was observed with isotonic saline injections), injected into the tumor center, half-way between the knee and ankle, and allowed to incubate for 3 days prior to iodide administration. Sodium iodide solution (at least 4.3 μg per mouse in 1 ml volume isotonic saline given intraperitoneally, i.p.) was administered to mice with either transduced A549 or untransduced A549 tumor xenografts (gene control). One milliliter of isotonic saline was given in place of iodide solution to the iodide controls. Approximately 30 min after iodide administration, mice were anesthetized for imaging using a mammography unit or mice were euthanased, and subsequently frozen, for either tissue sectioning or micro-computed tomography, micro-CT. Positive control studies in which mice with MCF-7 tumors were administered iodide. MCF-7 tumors were transplanted using the same procedure as A549 except mice with MCF-7 tumors ($n = 2$) were administered twice daily i.p. injections of estrogen (1 mg/mouse) for the duration of the study to promote tumor growth. MCF-7 and A549 tumors had similar growth kinetics.

Dog. The prostate of one mature male beagle (8.4 kg) was injected transrectally with 3×10^{-11} vp in 0.5 ml of isotonic saline under TRUS guidance. One day after viral injection, the dog was anesthetized using propofol (0.3 mg/kg/min, i.v. continuous infusion) while iodide as sodium iodide (660 mg) was administered intravenously to the dog over 1 h at a concentration of 20 mg/ml. The anesthetized dog was imaged with a spiral CT (Marconi Medical Systems, Cleveland, OH, USA) using a 3 mm slice and a 5 cm field of view, starting 3 h after iodide delivery stopped.

Whole animal radiographic images

To determine whether NIS expression and iodide accumulation could be radiographically detected, 4.3 μg iodine in isotonic saline was administered i.p to mice

DOI: 10.1002/cmmi

with A549 tumors transduced 3 days before with NIS. Approximately 30 min after iodide delivery, mice were prepared for macroscopic imaging, either anesthetized for immediate imaging with a clinical mammography unit ($n = 3$) or euthanased and frozen for subsequent micro-CT ($n = 3$). Mammographic images (24 kV, 71 mA s) were obtained on ketamine- (80 mg/kg, i.p.) and xylazine- (8 mg/kg, i.p.) anesthetized mice using a magnified field of view within an hour of iodide administration. Images from gene control mice given adenovirus lacking NIS were also obtained using the mammography unit ($n = 2$) and the micro-CT ($n = 2$). Dead mice imaged with micro-CT were immersed in degassed water and frozen (-20°C) prior to imaging. Details of the micro-CT equipment have been given previously(8) except for the CCD camera, TM9700 (PULNiX America Inc., Sunnyvale, CA, USA). In all cases mice were imaged while inside 50 ml plastic tubes (for anesthetized mice, tubes had air holes for mice to breathe). Images were analyzed as described in the Results section for radiographic contrast using ImageJ, shareware image processing software available from NIH at http://rsb.info.nih.gov/ij. Mammographic film images were digitized at 300 dpi to yield images 554×412 pixels with 8 bit grayscale. Four-hundred micro-computed tomography projection images per mouse were acquired at 681×572 pixels with 16 bit grayscale and slice reconstructed at either 256×256 pixels or 400×400 pixels, 16 bit grayscale with a 30×30 mm field of view.

Ex-vivo analyses

A549 tumors, MCF-7 tumors and normal gastrocnemius muscle were cryosectioned in their entirety. Adjacent slices were used to evaluate radiological contrast and the presence of NIS-expressing cells as well as iodide sequestration. Tissue sections were analyzed by: (1) immunohistochemistry for NIS expression from 10 μm thick slices on glass slides; (2) scanning electron microscopy, SEM, combined with X-ray spectrochemical elemental analysis from 100 μm-thick slices on acrylic plastic slides; or (3) high-resolution specimen radiographs for detection of cellular contrast from 100 μm thick slices on glass coverslips. Control studies included mice with A549 tumors given virus lacking NIS gene (gene control; $n = 2$), mice with A549 tumors given virus with NIS but not administered iodide (iodide control; $n = 2$), and as a positive control, MCF-7 tumors given iodide but no virus since they naturally express NIS ($n = 2$). For NIS detection, tissue sections were incubated with anti-NIS rabbit polyclonal antibody [1:1250; provided by S. Jhiang, Ohio State(9)] and donkey anti-rabbit Texas Red conjugated antibodies (1:500; Molecular Probes, Eugene, OR, USA) following standard procedures.(10) Briefly, the frozen tissue sections were fixed for 15 min in 3.7% formalin. Antibody was diluted and applied for 1 h at 37°C. BSA was used as a blocking agent to reduce nonspecific antibody binding. Following incubation with antibodies, slides were washed three times with room temperature DPBS. Cellular nuclei (DNA) were counterstained with 10 μg/ml 4′-6-diamidino-2-phenylindole (DAPI; Sigma-Aldrich Corp, Allentown, PA, USA) for 2 min. For the detection of iodide using elemental analysis, characteristic X-ray spectra were acquired at 100× magnification by SEM (JSM-840A, Jeol USA Inc., Peabody, MA, USA) and an integrated X-ray microanalyzer (IMIX, PGT, Princeton, NJ, USA). Tissues sections were sputtered with gold–palladium. Typical spectra were acquired using a probe current of 3×10^{-9} and 6×10^{-9} A, 100 s count time and approximately 1200 counts per second of characteristic X-rays. Specimen radiographs of tissue slices were acquired using a Hewlett-Packard Faxitron Cabinet X-ray System (43855A; HP Labs, Palo Alto, CA, USA; Faxitron X-Ray Corp., Wheeling, IL, USA) at 15kVp and 120 min exposures and silver halide high-contrast, high-resolution, ultra-flat glass photoplates (2506k1A, Microchrome Technology Inc., Reno, NV, USA). In the dark, glass coverslips with tissue sections were exposed to X-rays in groups of four as close to the X-ray source and as far from photoplates as possible to allow for maximum magnification of resultant images. Photoplates were immersed with gentle constant agitation in room-temperature tap water for 1 min, then developed with constant agitation in D-5 Developer (Microchrome Technology Inc., Reno, NV, USA) for 5 min at room temperature, rinsed for 1 min under constant agitation in room-temperature tap water, and fixed for 10 min in room-temperature F-4 Fixer (Microchrome Technology Inc., Reno, NV, USA). Plates were washed under room-temperature tap stream for 30 min and then dipped in solutions of increasing ethanol concentrations (20, 50, 70 and two changes of 100%). Subsequently, plates were allowed to air dry.

Data processing

Images were analyzed qualitatively for contrast. A visual comparison of contrast was made between tumors expressing NIS and control tissues either not expressing NIS or not administered iodide. No attempt was made to standardize contrast across imaging platforms or quantify images with respect to iodide concentration.

RESULTS

Microscopic concurrence of NIS expression, iodide sequestration and radiopacity

Antibody detection of NIS, radiographic contrast and high iodide concentration were measured microscopically

DOI: 10.1002/cmmi

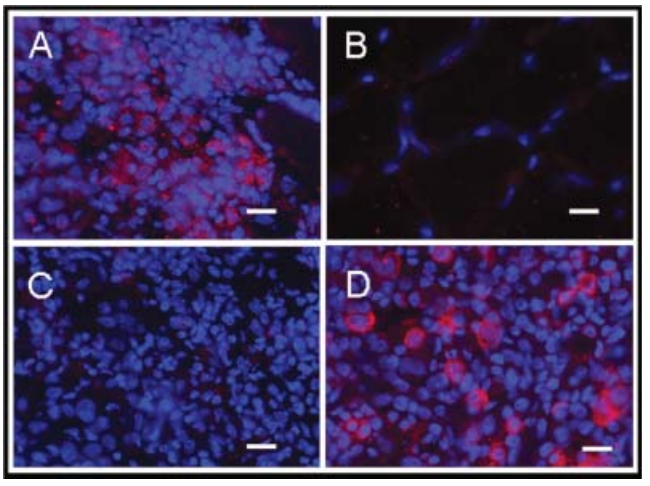

Figure 1. NIS protein expression in A549 human lung cancer xenografts transduced with adenovirus expressing NIS (A). NIS, shown in red, is distributed heterogeneously in regions of transduced A549 tumor cells. DAPI stained nuclei are shown in blue. In contrast, there is a lack of NIS expression observed in muscle cells from contralateral normal leg muscle (B) and A-549 tumor transduced with adenovirus lacking NIS (C). MCF-7 tumor, which exogenously and homogeneously expresses NIS (D), is included as a positive control. The white bars in the panels correspond to 25 μm.

in adjacent tissue slices in A549 tumor transduced with adenovirus-expressing NIS and control tissues (gene control: A549 tumor transduced with adenovirus lacking NIS; iodide control: A549 tumor transduced with adenovirus expressing NIS but no iodide administered; muscle control: normal gastrocnemius muscle from mouse administered systemic iodide; and as a positive control, MCF-7 tumor administered iodide). Figure 1(A) illustrates a region of A549 tumor that expressed NIS. An adjacent tissue slice showed a similar cluster of cells using high resolution X-ray techniques demonstrating distinct regions of radiological contrast that resembled individual cells [Fig. 2(A)]. Furthermore, iodide was identified at high concentration in an adjacent tissue slice using characteristic X-ray emission elemental analysis [Fig. 2(C)], supporting the contention that NIS-expressing cells sequestering iodide are responsible for the cells radiopacity. Microscopic concurrence of NIS expression, iodide sequestration and radiopacity was observed throughout tumor transduced with NIS.

In sharp contrast, there was a lack of NIS activity by immunohistochemical staining in control muscle [Fig. 1(B)] and in control tumor transduced with virus lacking NIS [Fig. 1(C)]. Adjacent control tissue sections containing cells not expressing NIS such as normal muscle and peripheral A549 tumor bordering muscle exhibited a lack of radiological contrast [Fig. 2(B)]. The strong iodide signal present in NIS-transduced A549 tumors was notably absent in A549 tumors lacking NIS assessed using X-ray elemental analysis [Fig. 2(C)]. In concordance with the NIS expressing A549 tumor, there was similar, although more uniform, NIS activity assessed by immunohistochemical staining in the positive control MCF-7 tumor [Fig. 1(D)] and corresponding evidence of iodide detected by spectrochemical elemental analysis in mice with MCF-7 tumor administered iodide [Fig. 2(C)]. In summary, tumors that expressed NIS were found to sequester iodide and presented with regions of radiographic contrast whereas tissue that did not express NIS did not contain iodide and did not exhibit regions of radiographic contrast.

Mouse whole-body imaging

As a proof-of-concept using standard diagnostic imaging devices, an attempt was made to detect X-ray contrast in mice with A549 tumors transduced with NIS and administered iodide systemically. Figure 3(A) shows an example of a typical radiograph of a mouse with a tumor expressing NIS and systemically administered iodide obtained using a clinical mammography unit. Two transverse cuts through the tumor are shown to illustrate (1)

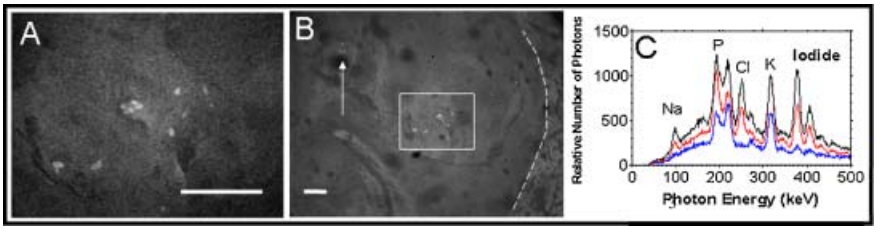

Figure 2. High resolution X-ray imaging and spectrochemical elemental analysis from adjacent slices of A549 tumor. (A) A typical specimen radiograph image. Individual radiopaque cells are clearly visible. The white bar in the panel corresponds to 100 μm. (B) A specimen radiograph with a larger field of view that includes multiple cellular clusters of radiopacity delineated by the box and the arrow. Tissue regions at the tumor periphery (the tumor–muscle boundary is delineated by the dashed line), and particularly in muscle, situated to the right of the dashed line, were void of cellular clusters of radiopacity. The white bar corresponds to 100 μm. (C) Representative scanning electron microscope elemental analysis X-ray spectra from mice administered systemic iodide with A549 tumor transduced with NIS (black line, upper curve), positive control, MCF-7 tumor (red line, middle curve) and A549 tumor not transduced with NIS (blue line, bottom curve). Peaks correspond to sodium (Na), phosphorus (P), chlorine (Cl), potassium (K) and iodide. Other unlabeled peaks correspond to gold and palladium which were used in the sample preparation, and other higher energy electron orbits of iodide.

DOI: 10.1002/cmmi

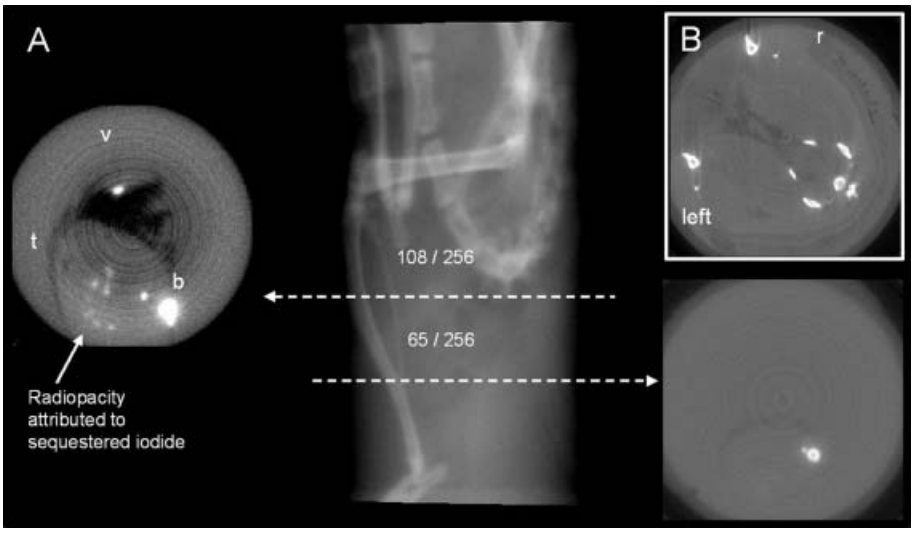

Figure 3. Micro-CT showing radiographic contrast in mice with A549 tumors expressing NIS. (A) A raw micro-CT projection and two reconstructed slices of a tumor transduced with NIS 3 days before given iodide (sodium iodide was given 30 min before the mouse was euthenased, frozen and the image acquired). Also shown are two reconstructed slices (256×256). The left tissue slice labeled 108 out of 256 cuts through the center of the tumor and illustrates typical subtle clusters of radiographic contrast attributable to iodide. Other regions of contrast are labeled t, b and v to denote tumor boundary, fibula and tibia leg bones, and tail vertebrae, respectively. Of note, radiographic contrast was only observed in the tumor core where the virus was injected and not at the tumor periphery, which was void of clusters of radiopacity. The dashed line cutting through the distal portion of the tumor, labeled 65 out of 256, corresponds to the right tissue slice with homogeneous radiographic contrast. (B) A representative example of homogeneous contrast throughout the slice of tumor which was transduced with virus lacking NIS. In the mouse shown, both legs had tumors implanted. It is of note that both the right leg (r) that received virus lacking NIS and the left leg (left) that did not receive virus showed no region of radiopacity despite the mouse having received a systemic injection of iodide.

clusters of contrast on the order of 4 mm in size and intensities 5–10% above average tumor values (using ImageJ) shown on the left in Fig. 3(A), and (2) absence of soft tissue contrast in peripheral tumor regions presumably not expressing NIS, shown on the right in Fig. 3(A). For comparison, similarly assessed radiographic contrast in control A549 tumors transduced with an adenovirus lacking NIS was homogeneous throughout the tumor region assessed macroscopically using film exposed with the conventional mammography unit [$n = 2$, example shown in Fig. 3(B)].

As a confirmatory study, mice with tumors expressing NIS and administered iodide and imaged using micro-CT exhibited clusters of increased radiographic contrast occupying up to a third of the tumor mass. Tumor boundaries were discernible in unprocessed raw images and were used to draw regions of interest around entire tumors. Consistently on micro-CT images (a typical example is shown in Fig. 4), the region of maximum contrast occurred at the site of viral injection (the slice in which tibia and fibula were maximally separated, i.e. approximately half-way between the knee and ankle). The region of contrast typically extended through 55 of 256 reconstructed slices, approximately 3.6 mm in length with at least 200 pixels (approximately 2×2 mm region of interest) in each slice having average contrast values 30% above average tumor values and some pixels exhibiting a maximum contrast value 60% above average tumor values (using ImageJ). As with the mammography unit, in contrast to the tumor expressing NIS in mice administered iodide, radiographic contrast assessed macroscopically using micro-CT in control A549 tumors transduced with a similar virus without NIS ($n = 2$) was homogeneous and typical of normal tumor values on both micro-CTs (Fig. 4). Similarly, contralateral normal muscle (Fig. 4) as well as A549 tumors transduced with NIS but not administered iodide ($n = 2$, not shown) exhibited uniform micro-CT radiocontrast throughout their tumor mass.

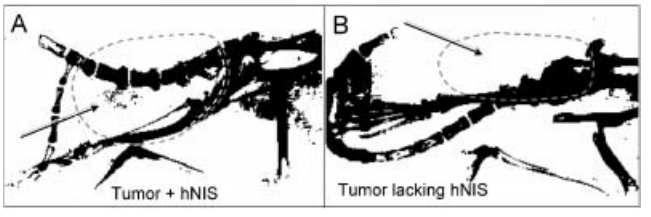

Figure 4. Radiographic contrast in live mice with A549 tumors expressing NIS showing representative X-ray attenuation images of mice obtained using a conventional mammography unit. The mice had A549 tumors injected with adenovirus containing NIS (A) and lacking NIS (B) three days before iodide was administered intraperitoneally. The corresponding images directly below illustrate those pixels whose values were greater than one standard deviation above the average tumor contrast. In this and all other studies, high-intensity pixels were only observed in the tumors expressing NIS (shown by the arrow in A). This is to our knowledge the first radiographic demonstration of gene expression imaged noninvasively in a live animal.

DOI: 10.1002/cmmi

Dog whole-body imaging

The dog study was included to assess the clinical utility of radiological NIS imaging. If feasible, our group and others using NIS as a reporter gene may consider adopting nonradioactive iodide/NIS imaging to monitor adenoviral gene expression. Our ongoing adenovirus-mediated suicide-gene therapy clinical trial targets prostate cancer; consequently we examined the ability to image NIS expression in a normal canine prostate using a clinical CT. Discerning image contrast in individual image slices was challenging because of low signal-to-noise ratio, requiring the summation of adjacent slices along the axis of symmetry and image processing. A pie-shaped region of contrast evident in the prostate of a living dog resembled the pattern of gene expression expected. Specifically, the pie-shaped glandular structure of the prostate has been clearly evident in previous studies using high-resolution images from autoradiographs of radioactive anion sequestered by NIS following the local injection of adenovirus [reported previously].(7,11) Figure 5 illustrates an example CT showing regions of radiopacity attributable to NIS expression in the prostate of an anesthetized dog. The dog study results suggests that CT imaging of nonradioactive iodide has limited potential value for large animal (i.e. human) imaging of gene expression persistence.

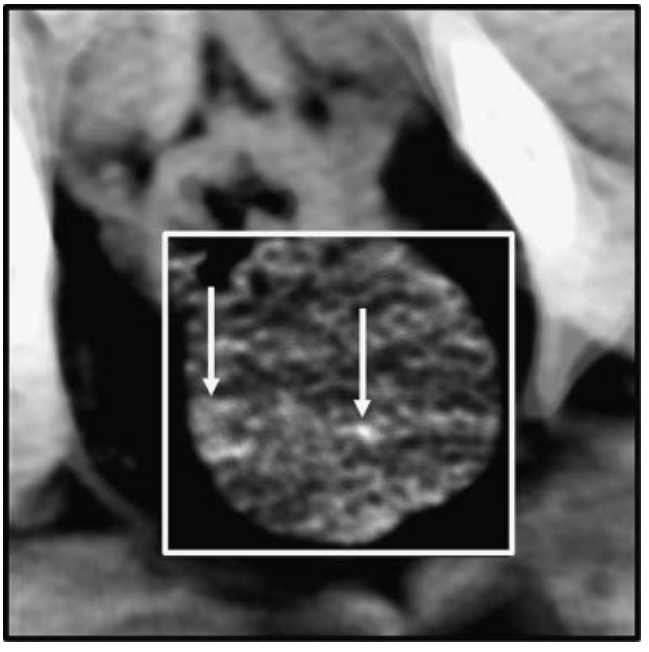

Figure 5. CT image of dog prostate transduced with hNIS. Two regions of contrast are barely noticable, shown by arrows. On the left is a region of contrast most intense at the periphery and extending along a pie-shape structure toward the urethra shown by the arrow on the right. The region bordered in white is contrast-enhanced such that gray levels between 28 and 49 were expanded to between 0 and 255. The prostate is approximately 9 cm^3 in volume (2–3 cm in diameter). The image represents the sum of four adjacent 2 mm slices. The study demonstrates that imaging NIS radiocontrast in large animals is challenging.

DISCUSSION

Reporter gene technology at present is based on the sequestration of radioactive tracers, fluorescent probes or MR contrast agents. Impediments to clinical translation include the perceived health risk of radioactive injectables, attenuation of optical signal limiting penetration of fluorescent photons through tissue to under a centimeter and the expense and limited accessibility of magnetic resonance imaging systems. Radiological attenuation has been universally adopted as the most widely used imaging procedure because of its safety, utility and cost. The same advantages should be considered in assessing radiological attenuation for reporter gene imaging.

In this report the potential of NIS sequestered nonradioactive iodide for monitoring gene expression is experimentally demonstrated. In homogeneous tissues, as with the small experimental animal tumors studied, the ability to monitor viral distribution and persistence with a simple planar X-ray is an attractive alternative to existing reporter imaging strategies. Radiographic contrast attributable to NIS gene expression was identified microscopically and macroscopically in mice using clinical radiological equipment. At high magnification the microscopic regions of high contrast had the size and shape of individual cells. The regions corresponded with localization of NIS assessed with an antibody to NIS and increased amounts of iodide were measured using an electron probe X-ray microanalyzer. Imaging contrast in the dog prostate was challenging, suggesting that the translation to routine clinical use may require higher levels of NIS than are achievable with a human virus in a dog or that higher levels of iodide are needed.

The transduction and subsequent expression of NIS gene into target tissue in order to sequester radioactive iodide and anions of similar size and charge have been examined experimentally in numerous pre-clinical studies. Link and co-workers(12) demonstrated that seven times the I-123 activity was localized to cells stably transduced with NIS using SPECT. Groot-Wassink and co-workers extended the studies to adenovirus biodistribution using PET imaging(13) and illustrated a linear relationship between the percentage injected iodide dose and the number of NIS-expressing adenoviral particles administered.(14) NIS-based gene imaging has been shown to be comparable to other gene imaging strategies in terms of sensitivity. For example, Shin *et al.*(15) showed that the signal per unit NIS mRNA ($=23\,000 \pm 4000$ cpm) of I-131/NIS was comparable to an iodinated TK substrate using gamma camera imaging. Recently, both NIS-expressing adenovirus used to sequester I-124 for PET imaging and I-123 for gamma camera imaging has been shown to sequester 7% of the

DOI: 10.1002/cmmi

injected iodide.(16) NIS imaging has the potential for monitoring gene expression in human gene therapy trials, as demonstrated by a recent feasibility study in large animals.(17) The nonradioactive technique as shown by the current results is sensitive enough for pre-clinical studies and further work is needed for quantification of the sensitivity prior to its use in human studies.

The potential advantages to using nonradioactive iodide for imaging compared with the use of radionuclide imaging with SPECT or PET are modest. First, nonradioactive iodide use in animals and human studies can be carried out without Radiation Safety Committee (RSC) regulatory control. RSC approval is not needed for externally applied radiographic imaging and is required for unsealed radioactive source use, so nonradioactive iodide-based imaging is simpler to use than techniques requiring radionuclides. Second, CT scanners are probably as accessible as nuclear medicine scanners at centers utilizing gene therapy strategies so imaging strategies designed to use CT rather than nuclear medicine have no inherent advantage with respect to their potential routine and widespread utilization. Third, the radiation dose from the nonradioiodide technique may be more or less than the dose from radionuclide-based techniques depending on the imaging field of interest. In summary, there is not a significant scientific advantage for using nonradioiodide over radionuclide strategies, however the present study demonstrates that nonradioactive iodide provides a complementary imaging tool for small animal studies.

Regardless of the detector used, radionuclides are probably orders of magnitude more detectable than nonradioactive iodide. Morris and co-workers demonstrated the difference in sensitivity surreptiously in their report, showing NIS gene expression was detectable using I-124 with PET whereas NIS gene expression was not readily detectable in the CT images.(16) Other human clinical evidence suggests that NIS expression is indeed detectable by CT scans under optimum conditions. For example, normal functioning thyroid tissue expresses NIS indigenously, sequesters iodide at about twice the concentration as tissue expressing exogenous NIS(7) and results in radiopacity between that of bone and muscle. The data presented in this report is the first demonstration that exogenous NIS and systemically administered iodide is sufficient for noninvasive imaging at least in small animals.

Two complications to the routine use of radiological attenuation for gene imaging are worth considering. First, the indigenous expression of NIS may complicate the interpretation of exogenous gene expression. Normal tissues that ordinarily express NIS include thyroid, salivary glands and lactating breast. It is not expected that these tissues would interfere with the measurement of NIS from gene therapy. On the other hand, some breast cancers have been shown to express NIS(18–20) and it could be assumed that sequestered iodide from indigenous NIS would interfere with the interpretation of NIS expression from gene therapy. It follows from the current study that radiopacity from a standard mammogram may in part be a consequence of sequestered iodide secondary to NIS expression. Further breast cancer studies are required to refute or confirm this hypothesis. Second, the presence of other structures of radiopacity may obscure the interpretation, especially microcalcifications. The solution is to obtain an image before as well as after iodide is administered and compare images to assure NIS activity is attributable to iodide sequestration. In summary we have demonstrated that radiographic contrast has potential to provide a useful and simple means to monitor exogenous gene expression.

Acknowledgements

The authors are grateful for the keen technical assistance of Kelly Ann Keenan and Chunhui Jiang. The authors also acknowledge the generous gift of NIS antibody by Sissy Jhiang, Ohio State University. The studies were supported by the National Institutes of Health, P01CA097012 (SOF).

REFERENCES

1. Prof. Roentgen's discovery. *Scientific American* (1845–1908) 8 February 1896; **LXXIV**(6).
2. Rontgen WC. Eine neue Art von Strahlen, presented to the secretary of the Würzburg Physical–Medical Society and available in English translation by Stanton A, On a new kind of rays. *Nature* 1896; **53**: 274–276.
3. Chantler CT. Theoretical form factor, attenuation and scattering tabulation for $Z = 1$–92 from $E = 1$–10 eV to $E = 0.4$–1.0 MeV. *J. Phys. Chem. Ref. Data* 1995; **24**: 71–643.
4. White DR, Booz J, Griffith R, Spokas JJ, Wilson IJ. *Tissue Substitutes in Radiation Dosimetry and Measurement*. ICRU Report 44 (International Commission on Radiation Units and Measurements, Bethesda, USA). Oxford University Press: Oxford, 1989; 1–189.
5. Dai G, Levy O, Carrasco N. Cloning and characterization of the thyroid iodide transporter. *Nature* 1996; **379**: 458–460.
6. Smanik PA, Liu Q, Furminger TL, Ryu K, Xing S, Mazzaferri EL, Jhiang SM. Cloning of the human sodium lodide symporter. *Biochem. Biophys. Res. Commun.* 1996; **226**: 339–345.
7. Barton KN, Tyson D, Stricker H, Lew YS, Heisey G, Koul S, de la Zerda A, Yin FF, Yan H, Nagaraja TN, Randall KA, Jin GK, Fenstermacher JD, Jhiang S, Ho Kim J, Freytag SO, Brown SL. GENIS: gene expression of sodium iodide symporter for noninvasive imaging of gene therapy vectors and quantification of gene expression *in vivo*. *Mol. Ther.* 2003; **8**: 508–518.
8. Reimann DA, Hames SM, Flynn MJ, Fyhrie DP. A cone beam computed tomography system for true 3D imaging of specimens. *Appl. Radiat. Isot.* 1997; **48**: 1433–1436.
9. Jhiang SM, Cho JY, Ryu KY, DeYoung BR, Smanik PA, McGaughy VR, Fischer AH, Mazzaferri EL. An immunohistochemical study of Na+/I− symporter in human thyroid tissues and salivary gland tissues. *Endocrinology* 1998; **139**: 4416–4419.
10. Castro MR, Bergert ER, Beito TG, Roche PC, Ziesmer SC, Jhiang SM, Goellner JR, Morris JC. Monoclonal antibodies against the human sodium iodide symporter: utility for immunocytochemistry of thyroid cancer. *J. Endocrinol.* 1999; **163**: 495–504.

11. Barton KN, Xia X, Yan H, Stricker H, Heisey G, Yin FF, Nagaraja TN, Zhu G, Kolozsvary A, Fenstermacher JD, Lu M, Kim JH, Freytag SO, Brown SL. A quantitative method for measuring gene expression magnitude and volume delivered by gene therapy vectors. *Mol. Ther.* 2004; **9**: 625–631.
12. Mandell RB, Mandell LZ, Link CJ Jr. Radioisotope concentrator gene therapy using the sodium/iodide symporter gene. *Cancer Res.* 1999; **59**: 661–668.
13. Groot-Wassink T, Aboagye EO, Glaser M, Lemoine NR, Vassaux G. Adenovirus biodistribution and noninvasive imaging of gene expression *in vivo* by positron emission tomography using human sodium/iodide symporter as reporter gene. *Hum. Gene Ther.* 2002; **13**: 1723–1735.
14. Groot-Wassink T, Aboagye EO, Wang Y, Lemoine NR, Reader AJ, Vassaux G. Quantitative imaging of Na/I symporter transgene expression using positron emission tomography in the living animal. *Mol. Ther.* 2004; **9**: 436–442.
15. Shin JH, Chung JK, Kang JH, Lee YJ, Kim KI, Kim CW, Jeong JM, Lee DS, Lee MC. Feasibility of sodium/iodide symporter gene as a new imaging reporter gene: comparison with HSV1-tk. *Eur. J. Nucl. Med. Mol. Imag.* 2004; **31**: 425–432.
16. Dingli D, Kemp BJ, O'Connor MK, Morris JC, Russell SJ, Lowe VJ. Combined I-124 positron emission tomography/computed tomography imaging of NIS gene expression in animal models of stably transfected and intravenously transfected tumor. *Mol. Imag. Biol.* 2006; **8**: 16–23.
17. Siddiqui F, Barton KN, Stricker HJ, Steyn PF, LaRue SM, Karvelis KC, Sparks RB, Kim JH, Brown SL, Freytag SO. Design considerations for incorporating sodium iodide symporter reporter gene imaging into prostate cancer gene therapy trials. *Hum. Gene Ther.* 2007; **18**: 312–322.
18. Tazebay UH, Wapnir IL, Levy O, Dohan O, Zuckier LS, Zhao QH, Deng HF, Amenta PS, Fineberg S, Pestell RG, Carrasco N. The mammary gland iodide transporter is expressed during lactation and in breast cancer. *Nat. Med.* 2000; **6**: 871–878.
19. Upadhyay G, Singh R, Agarwal G, Mishra SK, Pal L, Pradhan PK, Das BK, Godbole MM. Functional expression of sodium iodide symporter (NIS) in human breast cancer tissue. *Breast Cancer Res. Treat.* 2003; **77**: 157–165.
20. Rudnicka L, Sinczak A, Szybinski P, Huszno B, Stachura J. Expression of the Na(+)/I(−) symporter in invasive ductal breast cancer. *Folia Histochem. Cytobiol.* 2003; **41**: 37–40.

DOI: 10.1002/cmmi